CHANGES IN ANATOMICAL BRAIN CONNECTIVITY BETWEEN AGES 12 AND 30: A HARDI STUDY OF 484 ADOLESCENTS AND ADULTS

Emily L. Dennis[1], Neda Jahanshad[1], Arthur W. Toga[1], Kori Johnson[2,3], Katie L. McMahon[2], Greig I. de Zubicaray[4], Nicholas G. Martin[3], Ian Hickie[5], Margaret J. Wright[3,4], Paul M. Thompson[1]

[1]Laboratory of Neuro Imaging, UCLA School of Medicine, Los Angeles, CA, USA

[2]Center for Advanced Imaging, Univ. of Queensland, Brisbane, Australia

[3]Queensland Institute of Medical Research, Brisbane, Australia

[4]School of Psychology, University of Queensland, Brisbane, Australia

[5]Brain and Mind Research Institute, University of Sydney, Australia

ABSTRACT

Graph theory can be applied to matrices that represent the brain's anatomical connections, to better understand global properties of anatomical networks, such as their clustering, efficiency and "small-world" topology. Network analysis is popular in adult studies of connectivity, but only one study – in just 30 subjects – has examined how network measures change as the brain develops. Here we assessed the developmental trajectory of graph theory metrics of structural brain connectivity in a cross-sectional study of 484 subjects, aged 12 to 30. We computed network measures from 70x70 connectivity matrices of fiber density generated using whole-brain tractography in 4-Tesla 105-gradient high angular resolution diffusion images (HARDI). All network measures changed with age, and both *age* and age^2 effects were identified. The strongest age effect was seen for the normalized clustering (lambda), which decreased across development. HARDI-based connectivity maps are sensitive to the remodeling and refinement of structural brain connections as the human brain develops.

Index Terms – graph theory, high angular resolution diffusion imaging (HARDI), tractography, network analyses, development, structural connectivity

1. INTRODUCTION

The human brain changes profoundly as it develops. Classical anatomical studies show pruning of short-range connections throughout childhood, in favor of long range ones [1]. Diffusion imaging may also be combined with fiber tractography to reveal axonal pathways *in vivo*. In DTI studies, the fractional anisotropy of diffusion, which is sensitive to myelination, increases in childhood, plateaus in adulthood, and then declines in old age [2]. Defining the developmental trajectory for various aspects of brain structure is critical in determining how the brain normally develops. Normative statistics on brain connectivity are also useful to help identify anomalies of brain wiring that have been implicated in autism, schizophrenia, and other neurological and psychiatric disorders.

Graph theory, a branch of mathematics created to describe and analyze graphs, has recently been applied to characterize structural and functional networks computed from brain images [3]. Resting-state fMRI and MEG/EEG studies define connectivity in terms of correlations in time-series, for signals recorded from different parts of the brain. Recent high profile studies have estimated the "developmental ages" or relative maturity of subjects, based on resting-state data in children [4]. If diffusion images are collected, whole-brain tractography can be used to recover the density and integrity of tracts that interconnect pairs of brain regions. The topology and network properties of the resulting connectivity matrices can be summarized in terms of their characteristic path length (CPL), mean clustering coefficient (MCC), global efficiency (EGLOB), small-worldness (SW), and modularity (MOD) [5]. CPL measures a network's average path length - the minimum number of edges needed to travel from one node to another. MCC measures how many neighbors of a given node are also connected to each other, relative to the total possible number of connections in the network. EGLOB is the inverse of CPL; networks with lower CPL are more efficient. SW represents the balance between network differentiation and integration, calculated as a ratio of local clustering and characteristic path length of a node relative to the same ratio in a randomized network. MOD is the degree to which a system may be subdivided into smaller networks [6].

Network metrics have been fruitfully applied to brain networks [7] but only one study has investigated their developmental trajectory [8] – in only 30 subjects. Here we scanned a much larger sample of 484 subjects – aged 12 to 30 – with 4-Tesla 105-gradient diffusion imaging. We set out to determine which measures of structural brain connectivity change the most from late childhood to adulthood. We computed graph theory metrics, from whole-brain HARDI tractography, in children (12 years old), teenagers (16 years old) and adults (aged 20-30).

2. METHODS

2.1. Subjects and Image Acquisition

Participants were recruited as part of a 5-year research project scanning healthy young adult Australian twins with structural brain MRI and DTI [9]. We analyzed scans from 484 right-handed subjects (299 women/185 men, average age=21.4, SD=4.44). This population included 165 monozygotic (MZ) twins, 283 dizygotic (DZ) twins, and

36 non-twin siblings, from 285 families. 371 were adults, 60 were adolescents, and 53 were children. Whole-brain anatomical MRI and high angular resolution diffusion images (HARDI) were collected with a 4T Bruker Medspec MRI scanner. T1-weighted anatomical images were acquired with an inversion recovery rapid gradient echo sequence, with TI/TR/TE = 700/1500/3.35ms; flip angle = 8 degrees; slice thickness = 0.9mm, and a 256x256x256 acquisition matrix. Diffusion-weighted images (DWI) were also acquired using single-shot echo planar imaging with a twice-refocused spin echo sequence to reduce eddy-current induced distortions. Imaging parameters were: 23cm FOV, TR/TE 6090/91.7ms, with a 128x128 acquisition matrix. Each 3D volume consisted of 55 2-mm thick axial slices with no gap and 1.79x1.79 mm^2 in-plane resolution. 105 images were acquired per subject: 11 with no diffusion sensitization (i.e., T2-weighted b_0 images) and 94 diffusion-weighted (DW) images (b = 1159 s/mm^2) with gradient directions evenly distributed on the hemisphere. The HARDI scan took 14.2 min to collect.

2.2. Cortical Extraction and HARDI Tractography

Connectivity analysis was performed as in [10]. Briefly, non-brain regions were automatically removed from each T1-weighted MRI scan, and from a T2-weighted image from the DWI set, using the FSL tool "BET" (FMRIB Software Library, http://fsl.fmrib.ox.ac.uk/fsl/). A neuroanatomical expert manually edited the T1-weighted scans to refine the brain extraction. All T1-weighted images were linearly aligned using FSL (with 9 DOF) to a common space with 1*mm* isotropic voxels and a 220×220×220 voxel matrix. For each subject, the 11 eddy-corrected images (using FSL tool "eddy_correct" http://fsl.fmrib.ox.ac.uk/fsl/) with no diffusion sensitization were averaged, linearly aligned and resampled to a downsampled version of their corresponding T1 image (110×110×110, 2×2×2mm). Averaged b_0 maps were elastically registered to the structural scan using a mutual information cost function to compensate for EPI-induced susceptibility artifacts. 35 cortical labels per hemisphere, as listed in the Desikan-Killiany atlas [11], were automatically extracted from all aligned T1-weighted structural MRI scans using FreeSurfer (http://surfer.nmr.mgh.harvard.edu/). T1-weighted images and cortical models were aligned to the original T1 input image space and down-sampled to the space of the DWIs, using nearest neighbor interpolation (to avoid intermixing of labels). To ensure tracts would intersect cortical labeled boundaries, labels were dilated with an isotropic box kernel of size 5×5×5 voxels.

The matrix transforming the mean b_0 image to the T1-weighted volume was applied to each of the 94 gradient directions to properly re-orient the orientation distribution functions (ODFs). At each HARDI voxel, ODFs were computed using the normalized and dimensionless ODF estimator, derived for *q*-ball imaging (QBI). We performed HARDI tractography on the linearly aligned sets of DWI volumes using these ODFs, using the Hough transform method [12]. Elastic deformations obtained from the EPI distortion correction, mapping the average b_0 image to the T1-weighted image, were then applied to the tracts' 3D coordinates to accurately align the anatomy. Each subject's dataset contained 2000-10000 useable fibers (3D curves). For each subject, a full 70×70 connectivity matrix was created. Each element described the proportion of the total number of fibers connecting each of the labels; diagonal elements describe the total number of fibers passing through a certain cortical region of interest. Values were calculated as a proportion - normalized to the total number of fibers traced for each individual participant, so that results were not skewed by raw fiber count.

2.3. Graph Theory Analyses

On the 70x70 matrices generated above, we used the Brain Connectivity Toolbox (5; https://sites.google.com/a/brain-connectivity-toolbox.net/bct/Home) to compute CPL, MCC, EGLOB, SW, and MOD. We also generated 10 simulated random networks. The ratio of clustering coefficient in our network to the mean value obtained for a simulated random network was denoted by *lambda*. The ratio of CPL in our network to CPL in the simulated random network was denoted by *gamma*. All measures were calculated for the network as a whole, based on equations in [5].

In graph theory analyses, it is necessary to select a sparsity for the network, based on thresholding. Networks with a sparsity of 0.2 retain only 20% of the connections of the network computed from all available data. Completing analyses at a single sparsity level may be considered arbitrary, so we calculated network properties at multiple sparsities, and integrated the results across a specific range to generate more stable scores. We calculated the network measures for the whole brain over a range of sparsities (0.2-0.3, in 0.01 increments), and calculated the area under the plot spanned by those 11 data points to generate an integrated score for each measure. To determine at which sparsity these measures were most stable, we calculated them over the range 0-0.5, in 0.05 increments to assess these plots (see **Figure 1**). A sparsity higher than 0.3 is considered implausible for biological structural networks [13], and our plots show that the range 0-0.2 is unstable. We therefore selected the sparsity range 0.2-0.3 for our analyses.

2.4. Age Regression

Age effects on graph theory metrics of structural brain connectivity were estimated using the general linear mixed effects model, as well as two simpler linear mixed effects models, as follows:

$$\text{Graph theory metrics} \sim A + \beta_{age}\text{Age} + \beta_{sex}\text{Sex} + \beta_{TBV}\text{TBV} + \beta_{age,sex}\text{Age}\cdot\text{Sex} + \beta_{age^2}\text{Age}^2 + \alpha \quad \text{(Eq. 1)}$$

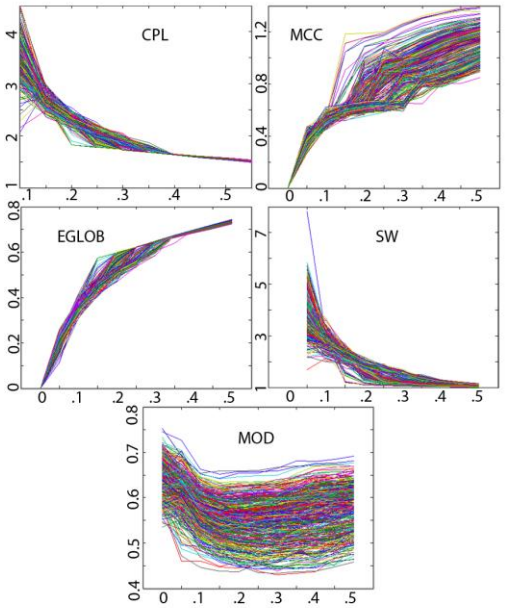

Figure 1. Values for 484 participants on 5 global measures across sparsity range 0-0.5 in 0.05 increments. Clearly, different sparsities affect the measures. The value for CPL at zero sparsity is infinite, and is omitted from the graph.

Graph theory metrics ~ $A + \beta_{age}Age +$ (Eq. 2)
$\beta_{sex}Sex + \beta_{age,sex}Age \cdot Sex + \beta_{TBV}TBV + \alpha$

Graph theory metrics ~ $A + \beta_{sex}Sex$ (Eq. 3)
$+ \beta_{TBV}TBV + \beta_{age^2,sex}Age^2 \cdot Sex + \beta_{Age^2}Age^2 + \alpha$

Here, "graph theory metrics" could be any of CPL, MCC, EGLOB, SW, MOD, *lambda*, or *gamma*. *A* is a constant for each regression model, the βs are the covariate regression coefficients, and α is a coefficient that accounts for random effects. Random effects were used to account for family relatedness. We modeled the other variables (age, sex, TBV, age^2) as fixed effects. TBV denotes total brain volume.

3. RESULTS

Beta coefficients and associated *p*-values for each element in the model from **Eq. 1** are shown in **Table 1**, including both age and age^2 as covariates. As we adjust for one covariate, the other tends to fit in the opposite direction. This is expected, as the age effect decelerates (plateaus in adulthood). Significant results are italicized, after correcting for multiple comparisons using the false discovery rate (FDR) method [14].

Beta coefficients and *p*-values for each element in the model from **Eq. 2 and 3** with age and age^2 in separate models are shown in **Table 2.** Significant results are italicized, corrected for multiple comparisons using FDR.

Table 1. Effects of Age and Age^2 (when both included in the model) on global brain connectivity measures.

	Age	**Age^2**
CPL	*-0.38 ($2.20x10^{-10}$)*	*0.0078 ($1.1x10^{-7}$)*
MCC	*0.37 (0.0023)*	*-0.0068 (0.02)*
EGLOB	*0.1 ($3.22x10^{-6}$)*	*-0.0020 (0.00019)*
SW	*-0.83 ($1.98x10^{-6}$)*	*0.016 (0.00012)*
MOD	0.042 (0.34)	$8.8x10^{-5}$ (0.93)
Lambda	*-1.31 ($5.3x10^{-9}$)*	*0.025 ($2.59x10^{-6}$)*
Gamma	*-0.18 ($7.2x10^{-10}$)*	*0.0036 ($4.40x10^{-7}$)*

Table 2. Results of regression with Age and Age^2 *separately* on global measures of connectivity.

	Age		**Age^2**
CPL	*-0.082 ($3.70x10^{-6}$)*		*-0.0013 (0.0034)*
MCC	*0.11 (0.0034)*		*0.0020 (0.036)*
EGLOB	*0.024 ($6.41x10^{-5}$)*		*0.00041 (0.0046)*
SW	*-0.20 (0.00014)*		*-0.0032 (0.011)*
MOD	*0.046 0.0012)*		*0.0011 (0.0019)*
Lambda	*-0.32 ($9.73x10^{-6}$)*		*-0.0048 (0.0067)*
Gamma	*-0.043 ($9.79x10^{-6}$)*		*-0.00062 (0.0099)*

When age and age^2 are considered separately, all network measures show significant changes with age. As participants age, CPL decreases, MCC increases, EGLOB increases, SW decreases, MOD increases, lambda decreases, and gamma decreases. **Figure 2** shows a scatterplot of CPL vs. age.

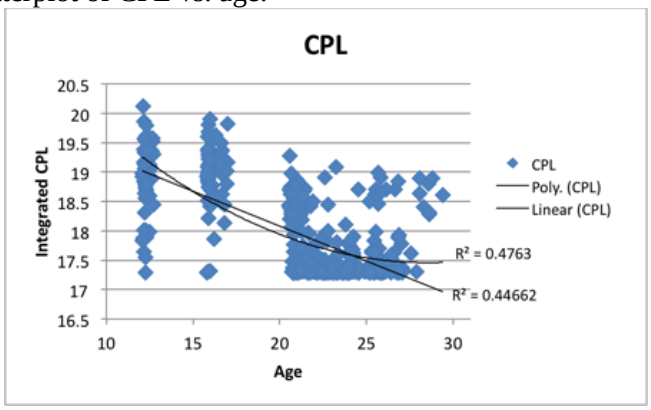

Figure 2. Scatterplot showing a negative, and non-linear, relationship between age and CPL.

For the sake of space, we only display this one graph, but the clear relationship shown here is representative of the scatterplots for the other 6 measures, for both age and age^2. For all measures, age effects are nonlinear, plateauing in adulthood. As expected from a model that plateaus, the beta coefficients for age and age^2 have opposite signs when combined in one model – after the linear effect of age is controlled for, the remaining variance has an opposite relationship with age^2. We also tested for age effects on each element in the original 70x70 fiber density matrices used to compute the graph theory metrics. We only tested connections present in >95% of our subjects. The *p* map generated from this analysis of age effects is shown in **Figure 3**. Age^2 generated a very

similar map, except for 5 connections: those with one terminus in the right precuneus and those with one terminus in the right insula.

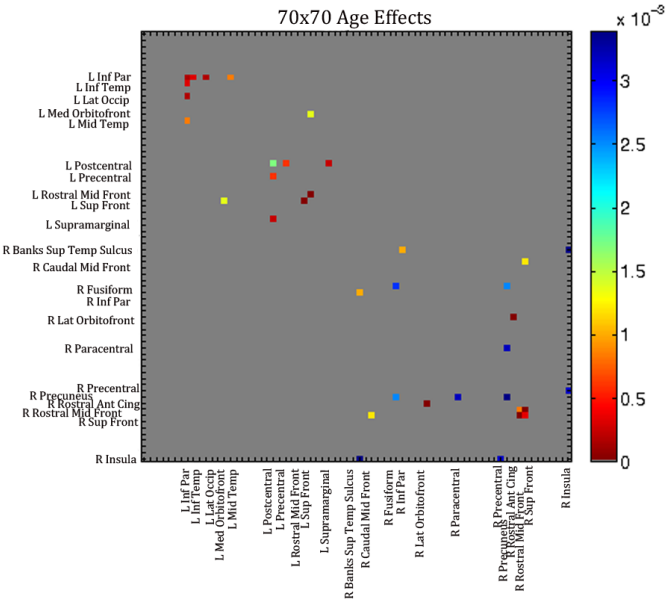

Figure 3. *P* map for fitted linear age effects on elements of the 70x70 fiber density matrix. Colors correspond to the *p* value as indicated. The overall map passes FDR.

4. DISCUSSION

We found non-linear relationships between age and a number of standard graph theory measures of brain structural connectivity. Measures of path length - both normalized relative to what would be expected in random networks (gamma) and unnormalized (CPL) - decreased non-linearly across development. Correspondingly, EGLOB increased non-linearly across development, which fits with the one prior study on this topic [8]. "Small-worldness" is calculated from the ratio of C/C_{rand} to L/L_{rand}, where C is the clustering in our network, C_{rand} is the clustering in a randomly generated network (in this case, the average from 10 randomly generated networks), L the path length in our network and L_{rand} the path length in the random network. C/C_{rand} is lambda, L/L_{rand} is gamma.

All subjects' structural networks showed a "small-world" network topology. Many graph theory metrics of connectivity are based on the small-world network model [3]. For a network with small world topology, gamma is around 1, and lambda is greater than 1 [7]. Both lambda and gamma decreased non-linearly across development. This decrease in path length (gamma), and the decrease in normalized clustering (lambda) may reflect the well-established process of pruning short-range connections over development [1]. Some connections are favored through experience, and are potentiated, while others are not reinforced, and are pruned. As short-range connections are pruned in favor of long-range ones, the number of paths necessary for information to travel between nodes decreases, increasing the network's efficiency. We also found an increase in modularity across development. Modularity reflects the degree of segregation within a network.

One limitation of the current study is the uneven sampling of different age groups, which was due to the availability of cohorts assessed at 12 and 16 but not in between. Nonparametric regression models may therefore be advantageous to derive empirical *p*-values for the fitted regression coefficients, but are unlikely to materially affect the conclusions given the strength of the age effects.

5. CONCLUSION

The period from adolescence to adulthood is marked by increases in the integration (or global efficiency) of structural networks, and increases in segregation, as seen in increased modularity. Regardless of age, the recovered brain networks showed a small-world topology. This study is a first step in developing statistical criteria for aberrant anatomical brain connectivity, or deviant trajectories of maturation, from childhood to adulthood.

6. REFERENCES

[1] Huttenlocher, Morphometric study of human cerebral cortex development. **Neuropsychologia**, 28:517-527, 1990.

[2] Kochunov et al., Fractional anisotropy of water diffusion in cerebral white matter across the lifespan. **Neurobiology of Aging**, 30:1149-1155, 2010.

[3] Sporns et al., Organization, development and function of complex brain networks. **Trends in Cogn Sci**, 8:418-425, 2004.

[4] Dosenbach et al., Prediction of individual brain maturity using fMRI. **Science**, 329:1358-1361.

[5] Rubinov & Sporns, Complex brain networks: graph theoretical analysis of structural and functional systems. **Nature Reviews Neuroscience**. 10:186-198, 2009.

[6] Bullmore & Bassett, Brain graphs: Graphical models of the human brain connectome. **Reviews in Advance**, 1-37, 2010.

[7] Bassett & Bullmore, Small-world brain networks. **The Neuroscientist**, 12(6):512-523, 2006.

[8] Hagmann et al., White matter maturation reshapes structural connectivity in the late developing human brain. **PNAS**, 107:19067-72, 2010.

[9] de Zubicaray et al., Meeting the challenges of neuroimaging genetics. **Brain Imaging and Behavior**, 2:258-263, 2008.

[10] Jahanshad et al., High angular resolution diffusion imaging (HARDI) tractography in 234 young adults reveals greater frontal lobe connectivity in women. **ISBI**, 2011. 1-5.

[11] Desikan et al., An automated labeling system for subdividing the human cerebral cortex on MRI scans into gyral based regions of interest. **NeuroImage**, 31:968-980, 2006.

[12] Aganj et al., A Hough transform global probabilistic approach to multiple-subject diffusion MRI tractography. **Med Image Analysis**, 15:414-425, 2011.

[13] Sporns, Networks of the Brain. The MIT Press, Cambridge, MA., 2011.

[14] Benjamini & Hochberg, Controlling the false discovery rate: a practical and powerful approach to multiple testing. **J R Stat Soc B**, 57:289–300, 1995.

ACKNOWLEDGMENTS

Supported by the NIH (R01 HD050735), and the National Health and Medical Research Council (NHMRC 486682, 1009064), Australia. Genotyping was supported by NHMRC (389875). Algorithm development was supported by NIH R01 grants EB008432, EB008281, EB007813 and P41 RR013642.